Graphite/nickel nanoparticle composites prepared by soft chemical methods

M. Victoria Bracamonte[1,2,†], Lisandro F. Venosta[1,2,†*], W. Gustavo Fano[3], Silvia E. Jacobo[4], Paula G. Bercoff[1,2.]

[1] Universidad Nacional de Córdoba, FAMAF, Ciudad Universitaria, Córdoba, Argentina

[2] CONICET, Instituto de Física Enrique Gaviola, Ciudad Universitaria, Córdoba, Argentina

[3] Laboratorio de Radiación Electromagnética (LRAD), Universidad de Buenos Aires, Facultad de Ingeniería, UBA, Buenos Aires, Argentina

[4] LaQuiMMAI-IQAI, Universidad de Buenos Aires, Facultad de Ingeniería, UBA, Buenos Aires, Argentina

***Corresponding author: venosta@famaf.unc.edu.ar**

† These authors contributed equally to this work

Abstract

The aim of this work is to obtain and characterize a composite material using an environmentally friendly matrix and green processes. To this end, different composites of as-received commercial graphite flakes (G) and nickel nanoparticles (Ni NPs) have been prepared by a one-step soft synthesis and by mechanical mixing. The properties of the composites have been compared by means of X-ray diffraction analysis, electron microscopy, Raman spectroscopy, and magnetometry. The microwave absorption behavior of the composites has also been assessed in the 0.1 to 3 GHz frequency range, to explore potential applications. The composites prepared by chemical synthesis followed by heat-treatment display improved crystallinity and magnetization. Small amounts of Ni NPs in the chemically synthesized composite not only enhance the microwave absorption properties of graphite, reaching values above 10 dB at 2.5 GHz, but also extend the use of graphite as a microwave absorber to low frequencies.

Keywords: graphite composites; Ni nanoparticles; electromagnetic properties

1. Introduction

Advances in technology have led to the development of a large number of electromagnetic (EM) devices for use in civil and military fields. In order to protect personnel from harmful EM interference, it is necessary to devise convenient devices with shielding and EM wave absorption

properties [1–5]. The main materials used for this application are composites consisting of a polymer bulk, such as an epoxy resin or silicone rubber, in some cases loaded with carbon particles [6–8], ferrites [9–11], magnetic metal powders [12, 13], or conducting polymers [14–16].

So-called "green" chemistry is based on the selection of environmentally friendly materials as well as on the reduction or elimination of hazardous reagents and solvents in the preparation processes [17]. There has been extensive research on Ni and other magnetic nanoparticle-based nanocomposites, and the synthesis of novel organometallic nanoparticles. Maleki et al. reported the synthesis of a solid-state hybrid catalytic system from organic precursors and inorganic oxides for selective conversions of alcohols and alkenes into aldehydes [18–30]. All of the prepared compounds showed catalytic properties. Among sustainable materials, carbon is one of the most abundant elements in the biosphere. Carbon-based materials have distinctive properties, such as low weight, processing benefits, flexibility, resistance to corrosion, and electrical properties that make them attractive for multiple applications [31–33].

Carbon materials for EM shielding mainly include carbon black, carbon fibers, carbon nanotubes, flexible graphite, graphene nanosheets, graphene oxide, or reduced graphene oxide, which are often produced through expensive, complicated, and usually difficult-to-scale processes, or natural graphite flakes (G). They have proven to be adequate for EM shielding at specific frequencies in the 8–12 GHz range, but not for low microwave frequencies (<5 GHz) [34, 35]. Wang et al. reported that crystalline graphite, without any further treatment, shows shielding effectiveness that is rather frequency-independent below 1 GHz and displays quite low values (<2 dB) [36]. When graphite is chemically oxidized under suitable conditions to form expanded graphite, it shows improved electrical conductivity, resulting in a very effective material for shielding purposes [37]. However, the synthesis conditions for expanding graphite are aggressive and require non-environmentally-friendly pre-treatments such as the use of strong acids (i.e., H_2SO_4).

According to Wang et al. [36], modified carbon nanotube (CNT) sheets are more effective in providing EM shielding compared to natural graphite and carbon black sheets in the frequency range from 0.015 to 1 GHz. However, because the cost of CNTs is high and they require complex fabrication techniques, it is a challenge to find alternative graphite-based materials with good shielding effectiveness (SE) in the low microwave frequency range. Although most of the carbonaceous materials used for EM shielding are chosen because of their electrical conductivity, the addition of magnetic nanoparticles is promising for enhancing absorption properties [4, 13, 38].

Spinel ferrites and magnetic metal nanoparticles have been widely studied, and have proved to be suitable materials for EM interference shielding applications over a wide range of frequencies, in particular at values of the order of 5 GHz [12, 38–44]. We have previously studied different single-phase spinel ferrites [45–48] as EM shielding materials, as well as composites combining soft and hard magnetic phases [49].

Panwar et al. [50] reported a polyethylene-graphite composite system. They presented shielding results in the ranges between 20 Hz and 5 MHz and between 1 GHz and 3 GHz, albeit without characterization details other than by SEM. A shielding value of about 50 dB could be mainly attributed to reflection. Pattanayak et al. [51] described a system consisting of dried banana leaves, making it interesting from an ecological perspective. They measured absorption in a frequency range between 1 and 20 GHz, and directly measured dielectric permittivity. Because the studied material was a dielectric, the magnetic contribution to microwave absorption was negligible. These authors attributed their good absorption result of 25 dB to dipole oscillations occuring at the interfaces between the microparticles of organic powder, producing heat dissipation. Wu et al. [52]

studied a paste composite of stainless steel fibers of 8 μm in diameter and 6 mm in length with 5 μm graphite flakes. In measurements at a single frequency of 1 GHz, they obtained a shielding effectiveness of 34 dB, although no basic characterization of the composite material was presented. Reflections produced by the metallic fiber component and its ferromagnetic character made the main contributions to shielding. These researchers highlighted the role of the graphite flake suspension as a key factor in enhancing the shielding efficiency of the material. Liu et al. [53] studied a system composed of micro flakes of expanded graphite with graphene oxide. The presented synthesis method was considered simple, environmentally friendly, and cost-effective. The authors obtained high values of shielding efficiency (between 35 and 53 dB), which were almost frequency-independent in the range between 8 and 12 GHz (X-band). The main shielding mechanism in this case was reflection, due to the conductive character of the composite.

In this context, the aim of this work has been to improve the microwave absorption properties of commercial graphite flakes by decoration with nickel nanoparticles and to study the response of the composite to EM radiation in a rarely studied frequency range. To achieve these goals, a composite material based on as-received commercial graphite flakes without further treatment (G) and nickel nanoparticles (Ni NPs) was produced by a one-step soft synthesis. Small amounts of Ni NPs were used (5 wt.%) in order to avoid clustering and/or agglomeration on the surface of the graphite flakes. The obtained products were characterized and then tested for EM shielding, giving satisfactory results at frequencies at which EM shielding results for such materials have rarely been reported, from 0.1 to 3.0 GHz.

2. Materials and methods

2.1 Synthesis and sample preparation

Ni NPs were prepared through a modified reduction method with borohydride [54–56]. Briefly, $NiCl_2$ (0.05 mol) was dissolved in 1 M HCl (50 mL). The mixture was stirred for 20 min at 25 ºC until complete dissolution of the metal chloride. Thereafter, 1 M aqueous $NaBH_4$ solution (50 mL) was added dropwise under vigorous stirring. During the reaction [Eq. (1)], bubbles were observed in the solution corresponding to H_2 production, while a black precipitate was formed.

$$2Ni^{2+}\,(aq) + 4BH_4^-\,(aq) + 12H_2O\,(l) \rightarrow 2Ni\,(s) + 14H_2\,(g) + 4B(OH)_3\,(aq) \qquad (1)$$

Once the reaction was complete (ca. 20 min), the obtained solid was collected by filtration and washed with doubly-distilled water and acetone. Finally, the product was dried in vacuo at 50 ºC for 18 h. Heat treatments of the as-prepared NPs were carried out under a dynamic vacuum in a quartz tube. Samples were calcined at 500 ºC for 1 h and then allowed to cool to room temperature, also in vacuo. **Figure 1** shows a schematic representation of the synthesis procedure.

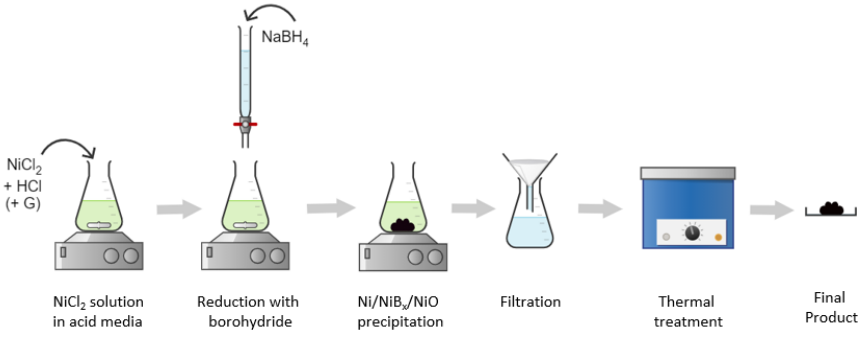

Figure 1. Scheme showing the synthetic route to Ni NPs and the composite G//Ni.

Graphite flake/Ni NP composites (denoted as G//Ni) were prepared by the same method as used for Ni NPs, adding 0.3 g of as-received graphite flakes G (>300 mesh, purchased from Sigma-Aldrich). After precipitation of the Ni NPs, the product was carefully washed and the resulting powder was dried in vacuo at 50 ºC for 18 h. One part of the G//Ni sample was calcined in vacuo at 500 ºC for 1 h and then allowed to cool to room temperature, also in vacuo. The resulting material was designated as G//Ni-TT.

In order to compare the properties of the chemically synthesized composite with a physical mixture of graphite and Ni NPs, a sample containing the same proportions of these components was prepared by milling for several minutes in an agate mortar. This sample was labeled as G+Ni.

2.2 Sample characterization

XRD patterns were measured with a Philips PW1800/10 diffractometer operated at an applied voltage of 40 kV and a current of 30 mA, equipped with a Cu-K_α radiation source. Scanning electron microscope (SEM) images were obtained with a Sigma Zeiss FE-SEM, operated at a working voltage of 5 kV. Transmission electron microscope (TEM) images were obtained with a high-resolution Hitachi HT7700 instrument, operated at 100 kV. The mean particle sizes of the Ni NPs and graphite flakes were statistically determined from SEM or TEM images.

Raman spectra were measured with a confocal Horiba Jobin–Yvon Labram HR spectrometer, with a laser wavelength of 514 nm. A Lake Shore 7300 vibrating sample magnetometer (VSM) was used to measure magnetization vs. applied field curves in the range ±1.3 T at room temperature.

To measure their electromagnetic properties, the synthesized powders were mixed with epoxy resin (ca. 30%) and hardener (ca. 20%) in ca. 50 wt.% fraction. Each sample was placed in a ring-shaped silicon mold and dried at room temperature for 48 h. The dimensions of the rings were determined by the characteristics of the sample holder, giving inner and outer diameters of 5.5 mm and 12.5 mm, respectively, and a thickness of 3.5 mm.

EM measurements were performed on a vector network analyzer (VNA) in the frequency range between 0.1 and 3.0 GHz, using the experimental set-up depicted in **Figure 2**. After calibration of the VNA, waveguide adapters were connected to the cylindrical sample holder containing the sample, and the *S* parameters (described below) were measured for each graphite composite.

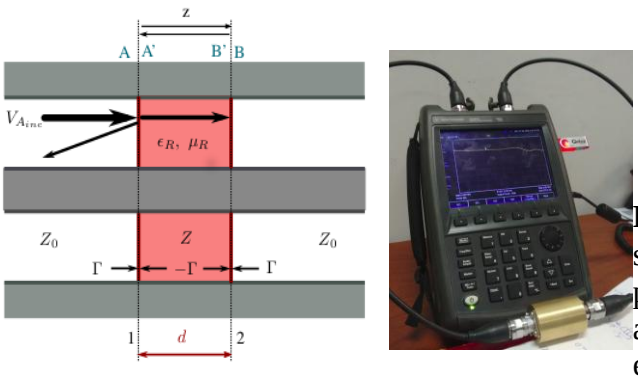

Figure 2. Schematic representation of the two air–sample interfaces when a sample of thickness *d* is placed inside a coaxial transmission line [57] (left) and photograph of the sample holder and equipment used in this work (right).

The measured *S* parameters S_{11} and S_{21} are related to reflectance (*R*) and transmittance (*T*), respectively, based on the following expressions [58]:

$$T = \left|\frac{E_T}{E_I}\right| = |S_{21}|^2 \quad (2a)$$

$$R = \left|\frac{E_R}{E_I}\right| = |S_{11}|^2 \quad (2b)$$

where E_I, E_T, and E_R are the incident, transmitted, and reflected electric fields of the wave, respectively.

Once the *S* parameters are measured, the *R* and *T* coefficients can be calculated using Eqs. (2), and these are used to obtain the absorbance $A = 1 - R - T$. The relative intensity of the effective incident EM wave within the material after reflection is based on the quantity 1–*R*. Therefore, the *effective absorbance* A_{eff} can be defined as: $A_{eff} = A/(1 - R)$.

Once the *transmittance* and *absorbance* parameters are obtained, the *reflection contribution* SE_R and *absorption contribution* SE_A parameters can be calculated using the following expressions:

$$SE_R = -log_{10}(1 - R) \quad (3a)$$

$$SE_A = -10log_{10}(1 - A_{eff}) = -10log_{10}\left(\frac{T}{1-R}\right) \quad (3b)$$

Hence, the values of the EM *shielding effectiveness* SE_T of the samples are determined by adding the contributions of SE_R and SE_A [59]:

$$SE_T = -10log_{10}(T) \quad (4)$$

3. Results and discussion

3.1 XRD

Figure 3 shows the measured XRD patterns obtained for the graphite and Ni NP composites without and with thermal treatment (G//Ni and G//Ni-TT, respectively), the physical mixture of graphite and Ni NPs (G+Ni), and pure Ni NPs. In each case, the peak intensities were normalized to the Ni (111) Bragg reflection. The reflection planes corresponding to graphite and Ni are indicated in the topmost pattern. Characteristic peaks of graphite corresponding to planes (002), (004), and (110) appear at the same positions for all of the samples. Ni NPs have an *fcc* structure, according to PDF file no. 96-210-2273. The peaks at positions 2θ = 44.35°; 51.67°, and 76.10° belong to the family of Ni planes (111), (002), and (022), respectively. For the Ni NPs and G//Ni-TT, no other phases, such as oxides or impurities, were observed within the detection limits of this technique. In the absence of thermal treatment, an extra peak at 43.36º was detected, attributable to the (200) reflection of NiO, which may have been formed during the synthesis process.

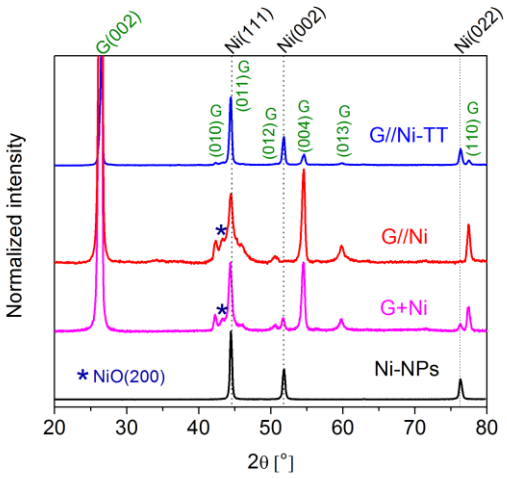

Figure 3. XRD patterns of G//Ni-TT, G//Ni, G+Ni, and Ni NPs. The reflection peaks of graphite are indexed as G(*hkl*) in the topmost diagram, while the vertical dashed lines are drawn as a guide, showing the positions of the Ni reflection planes (111), (002), and (022).

3.2 Electron microscopy

Figure 4a shows an SEM image of the as-received graphite flakes with the characteristic laminar structure and a mean particle size of 12 ± 5 µm. **Figures 4b**–**d** show TEM images of Ni NPs, G//Ni, and G//Ni-TT, respectively. From these results, it can be seen that the synthesis method produced spherical Ni NPs with a mean particle size of 24 ± 8 nm after heat treatment at 500 °C. The crystal size estimated using the Scherrer formula is ca. 26 nm, indicating that single-crystal particles were obtained.

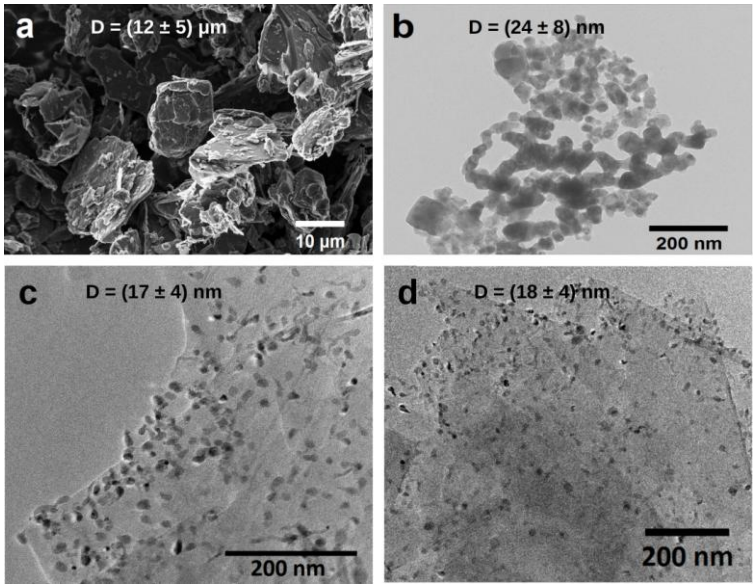

Figure 4. (a) SEM image of graphite. TEM images of (b) Ni NPs, (c) G//Ni, and (d) G//Ni-TT. The mean size *D*, calculated from size histograms of the particles (not shown), is displayed in each respective image.

According to TEM images, the Ni NPs had a mean particle diameter of 18 ± 4 nm and were homogeneously dispersed on the surface of the graphite. The image of the G//Ni-TT sample (**Figure 4d**) displays a similar particle size to that of G//Ni, indicating that the selected temperature was sufficient to enhance crystallinity without promoting grain growth. The larger Ni NP size in the absence of the graphite substrate (Ni NPs in **Figure 4b**) is due to sintering during the heat treatment. When Ni NPs are bonded to the graphite flakes and are well dispersed on the surface, they cannot grow at the expense of neighboring particles.

3.3 Raman spectroscopy

The Raman spectra of the G//Ni-NPs composites, measured with a 514 nm wavelength laser beam, are shown in **Figure 5**. The characteristic graphite bands D, G, and 2D can clearly be distinguished at 1355, 1582, and 2709 cm^{-1}, respectively. The inset in **Figure 5** shows the fitting of the D-bands for each sample, displaying a slight shift towards higher frequencies in the chemically treated samples, as compared to sample G (a vertical dashed line is drawn as a reference). It is known that the frequency of the D-band is a function of the defects in a sample, of its stress, and also of its electrical properties [60–62]. A slight shift is evident for the chemically treated samples, suggesting that during the synthesis process at least some of these characteristics of the composite are modified. Among them, a change in the electrical properties may occur, which could have an impact on the interaction mechanism between EM waves and the material.

Therefore, the shift in the D-band may be related to a change in the electronic behavior throughout the sample due to a more intimate contact between the Ni NPs and the graphite flakes, as reported by Kumar et al. [63]. It is important to note that the graphitic characteristics remain unchanged, taking into account the positions and shapes of the G- and 2D-bands, so that no amorphization, nor significant oxidation, occur in the samples during chemical treatment or mechanical mixing with Ni NPs.

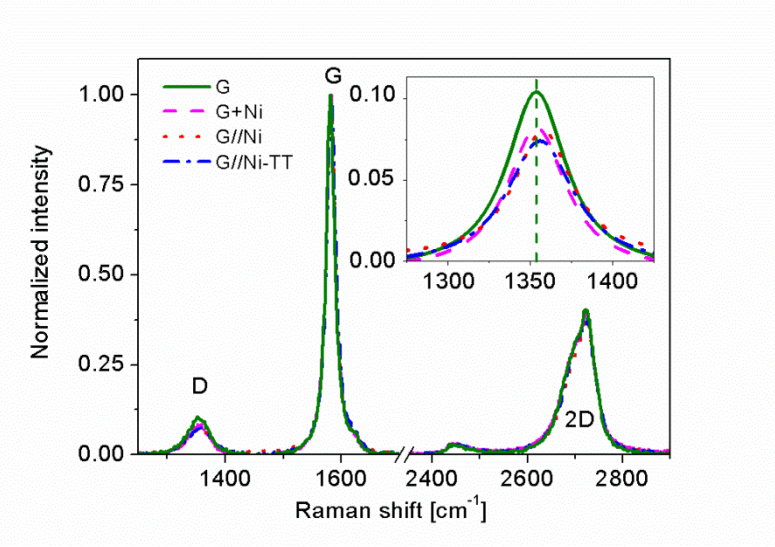

Figure 5. Normalized Raman spectra of the samples: G (green solid line), G+Ni (magenta dashed line), G//Ni (red dotted line), and G//Ni-TT (blue dash-dotted line). The inset shows the Lorentzian fitting of the D-bands. The vertical dashed line is drawn as a reference, at the corresponding position of the graphite D-band.

3.4 Magnetic properties

Hysteresis loops of the magnetic samples were measured on a VSM at room temperature. The inset in **Figure 6** shows the M vs. H curve of the Ni NPs, displaying the typical profile of a ferromagnetic material. Saturation magnetization, Ms=35 emu/g, is reached at low applied magnetic fields, as befits very soft magnetic behavior. The low Ms (compared to the bulk material value of 55 emu/g) is expected for a nanoparticulate system, in which the increment of the surface/volume ratio causes a decrease of Ms due to the increase in spin-disordered layers, i.e., a canting effect [64, 65].

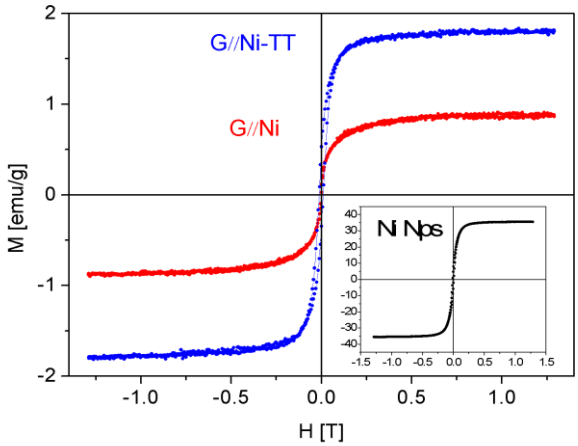

Figure 6. Hysteresis loops of the composites G//Ni and G//Ni-TT, measured at room temperature. The inset corresponds to the loop measured for Ni NPs.

Figure 6 shows that both G//Ni and G//Ni-TT are ferromagnetic. The sample without heat treatment (G//Ni) has a lower Ms compared to the heat-treated one (G//Ni-TT). This can be understood by considering the presence of some volatile residual remnant in the sample after the synthesis and/or the low crystallinity of the untreated Ni NPs. Whatever the cause may be, it is remedied by heat treatment. Using the value of Ms determined for Ni NPs, the amount of Ni present in sample G//Ni-TT was calculated as around 5 wt.%. Thus, the XRD and VSM results indicate that heat treatment is necessary in order to improve the structure and magnetic properties of the samples.

The coercive field Hc of sample G//Ni is 3 mT, which increases to 13 mT for G//Ni-TT, in good agreement with values reported by He and co-workers for similar single-domain Ni particles [64, 66].

3.5 EM shielding

The main mechanism of EM interference shielding is usually reflection. This mechanism is favored by the presence of mobile charge carriers (electrons or holes), which interact with the EM field during radiation. For this reason, it is desirable that a shielding material has good electrical conductivity. Metals mainly protect from EM interference by means of reflection, making them inappropriate for applications where EM absorption is required.

On the other hand, absorption is considered a secondary mechanism of EM shielding. In order to achieve significant absorption of the radiation, a material should have electric and/or magnetic dipoles that can interact with the incident wave.

In the prepared graphite/Ni NP composites, magnetic dipoles may be provided by the magnetic Ni NPs. **Figure 7** shows the behavior of the calculated shielding, due to both reflection SE_R (R) and absorption SE_A (A), for the prepared composites as a function of frequency. Both shielding contributions (R and A) increase with frequency in most of the samples.

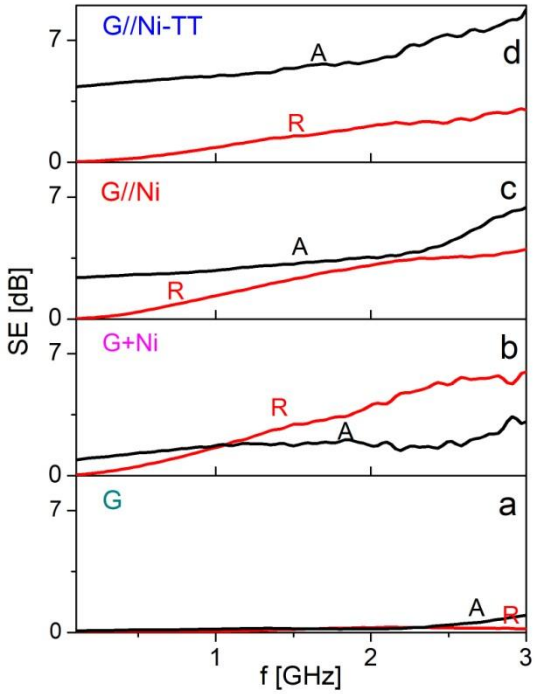

Figure 7. Shielding behavior of samples G, G+Ni, G//Ni, and G//Ni-TT (a, b, c, and d, respectively) in the frequency region 0.1–3.0 GHz. Reflection (R) and absorption (A) contributions for each sample are calculated according to Eqs. (3).

It is interesting to assess the different contributions (R and A) to shielding for each sample. It is known that the main shielding mechanism of graphite is the reflection contribution, due to its good conductivity. In the studied frequency range, however, both the reflection and the absorption in sample G display very low values, resulting in high transmission of electromagnetic radiation (**Figure 7a**). This result can be attributed to the fact that the shielding behavior of graphite is negligible in the low-frequency range, as previously reported by Wang et al. in the range 200–1000 MHz and by Koledintseva et al. in the range 1–3 GHz [36, 67].

The mechanical addition of metal NPs to graphite (sample G+Ni) improves both reflection and absorption in comparison to pure graphite (**Figure 7b**). However, R (SE_R) is the main contribution in this case, as absorption remains essentially constant throughout the explored frequency range. This effect may be ascribed to the presence of scattered Ni NPs in the graphite matrix, even when their loading is only 5 wt.%.

Figure 7c shows that the addition of Ni NPs to the graphite flakes by a chemical route not only increases the absorption capability (SE_A) of the G//Ni composite as compared to G+Ni (**Figure 7b**), but also makes this the most important contributor to the shielding effect. This behavior may probably be related to a modification of the graphite matrix, which acts as a support for the Ni NPs and prevents their agglomeration (**Figure 4c**). Ni NPs with an average size of 17 nm on the graphite flakes provide a large surface area that favors absorption through magnetic interaction with EM radiation. Huang and co-workers also observed that the inclusion of magnetic nanoparticles in a composite material based on functionalized carbon nanotubes increased the shielding effect at low frequencies [68].

The absorption properties of sample G//Ni-TT are displayed in **Figure 7d**. The reflection contribution is similar to that observed in sample G//Ni (**Figure 7c**), but absorption is considerably enhanced following the thermal treatment. This behavior can be interpreted in terms of an increase in crystallinity and hence an enhancement of the magnetic properties due to heat treatment, which is supported by the above-described XRD and magnetization results.

The total shielding effectiveness (SE_T) for each of the studied samples, calculated according to Eq. (4), is shown in **Figure 8**. It is remarkable that the incorporation of Ni NPs, even at very low concentrations, improves the behavior of the pure graphite flakes at low frequencies. In sample G//Ni-TT, SE_T reaches values above 10.0 dB at 2.6 GHz. At this frequency, the partial contributions to SE_T are reflection at 2.5 dB and absorption at 7.5 dB, evidencing the intrinsic importance of absorption in this composite. This result implies that sample G//Ni-TT is a feasible and competitive alternative among the current absorbing materials for use in the studied frequency range.

In order to further enhance the interaction mechanism of sample G//Ni-TT with radiation, we are currently conducting experiments with variable Ni contents on graphite flakes.

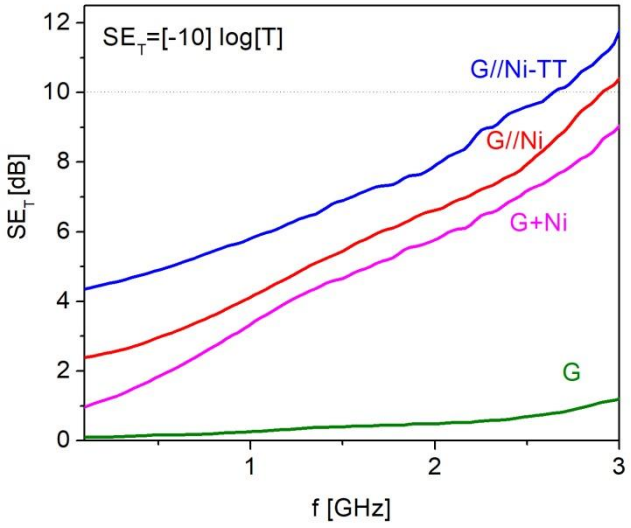

Figure 8. Total shielding effectiveness (SE_T) of the studied samples in the frequency region 0.1–3.0 GHz, calculated according to Eq. (4).

For the above-mentioned reasons, the relevance of the heat treatment in the performance of the synthesized composites as shielding materials is clear. However, any thermal treatment carried out at above 700 °C would destroy the carbon matrix in the graphite composites, and therefore the composite itself, since the burning temperature of carbon would be exceeded. Therefore, it is important to keep the temperature of the thermal treatment well below this value. Sample G//Ni-TT attenuates microwave radiation by over 90% above 2.5 GHz, so this composite has the best performance as an absorber among those assessed in this work. In the studied composites, the addition of Ni NPs plays a fundamental role in the absorption of electromagnetic radiation, especially at low frequencies.

The electromagnetic absorption at microwave frequencies is associated with the macroscopic behavior of the material. The wavelength of this radiation is much greater than the size of the grains and magnetic domains, and therefore the wave can only affect the bulk properties of electric and magnetic permittivity and their associated losses. The parameter responsible for the EM wave dissipation is called the attenuation coefficient, which depends on electric and magnetic properties, and these are a function of frequency. The presence of small and well-dispersed Ni NPs in the composite generates a higher EM wave scattering within the material, creating a larger number of interfaces, which facilitates polarization between surfaces as an absorption mechanism [63].

4. Conclusion

Composites of commercial graphite and Ni NPs have been prepared by mechanical mixing and chemical synthesis using environmentally friendly processes. Raman spectroscopy has confirmed that the graphite matrix remains unchanged in all of the prepared composites, even in G//Ni-TT, indicating that the thermal treatment does not disrupt the graphitic characteristics. Despite the low temperature of the thermal treatment, enhancements in the crystallinity and the magnetic properties of Ni NPs are observed. The one-step chemical process produces a homogeneous dispersion of Ni NPs on the graphite flakes, as confirmed by TEM images.

The composites present different EM properties in the frequency range 0.1–3.0 GHz depending on the preparation method. Although the inclusion of Ni NPs by physical mixing enhances the total shielding effectiveness SE_T, the chemical synthesis followed by heat treatment provides better results by significantly increasing the contribution of EM absorption. This behavior may be related to the presence of dispersed Ni NPs, an improvement in the crystallinity of the particles due to the thermal treatment, and more interactions between the particles and the graphite matrix because of the chemical preparation. The present study has revealed that the composite G//Ni-TT is a good candidate for shielding EM radiation, even with only a small wt.% of Ni NPs therein. Further experiments involving the addition of different amounts of Ni NPs to graphite are in progress. Some open questions related to the microwave shielding remain: one of them is how the surface area and pore size distribution of graphite affect the performance of the composites and how this is modified by decoration with Ni nanoparticles. These issues may be addressed in future work.

Acknowledgements

The authors acknowledge partial financial support for this research by the SeCyT (Universidad Nacional de Córdoba), CONICET (Argentina), and UBACyT. Dr. Bracamonte is especially grateful to the grant program BID-Foncyt (PICT-2016-0718).

References

1 H. Sun, R. Che, X. You, Y. Jiang, Z. Yang, J. Deng, L. Qiu, H. Peng, Cross-stacking aligned carbon nanotube films to tune microwave absorption frequencies and increase absorption intensities, Adv. Mater. 26 (2014) 8120-8125.

2 B. Wen, M. Cao, M. Lu, W. Cao, H. Shi, J. Liu, X. Wang, H. Jin, X. Fang, W. Wang, Reduced graphene oxides: light-weight and high-efficiency electromagnetic interference shielding at elevated temperatures, Adv. Mater. 26 (2014) 3484-3489.

3 D. X. Yan, H. Pang, B. Li, R. Vajtai, L. Xu, P. G. Ren, J. H. Wang, Z. M. Li, Structured reduced graphene oxide/polymer composites for ultra-efficient electromagnetic interference shielding, Adv. Funct. Mater. 25 (2015) 559-566.

4 G. Wang, Z. Gao, G. Wan, S. Lin, P. Yang, Y. Qin, High densities of magnetic nanoparticles supported on graphene fabricated by atomic layer deposition and their use as efficient synergistic microwave absorbers, Nano Res. 7 (2014) 704-716.

5 W. Zhang, Y. Xu, L. Yuan, J. Cai, D. Zhang, Microwave absorption and shielding property of composites with FeSiAl and carbonaceous materials as filler, J. Mater. Sci. Technol. 28 (10) (2012) 913-919.

6 D. Micheli, A. Vricella, R. Pastore, M. Marchetti, Synthesis and electromagnetic characterization of frequency selective radar absorbing materials using carbon nanopowders, Carbon 77 (2014) 756-774.

7 X. Sun, J. He, G. Li, J. Tang, T. Wang, Y. Guo, H. Xue, Laminated magnetic with enhanced electromagnetic wave absorption properties, J. Mater. Chem. C 1 (2013) 765-777.

8 X. Zhang, G. Ji, W. Liu, B. Quan, X. Liang, C. Shang, Y. Cheng, Y. Du, Thermal conversion of an Fe_3O_4@metal–organic framework: a new method for an efficient Fe–Co/nanoporous carbon microwave absorbing material, Nanoscale 7 (2015) 12932-12942.

9 T. Liu, Y. Pang, H. Kikuchi, Y. Kamada, S. Takahashi, Superparamagnetic property and high microwave absorption performance of FeAl@(Al, Fe)$_2O_3$ nanoparticles induced by surface oxidation, J. Mater. Chem. C 3 (2015) 6232-6239.

10 H. M. Xiao, X. M. Liu, S. Y. Fu, Nanomaterials: synthesis, characterization, and applications, Compos. Sci. Technol. 66 (2006) 2003-2008.

11 M. Meshram, N.K. Agrawal, B. Sinha, P. Misra, Characterization of M-type barium hexagonal ferrite-based wide band microwave absorber, J. Magn. Magn. Mater. 271 (2004) 207-214.

12 F. Wen, F. Zhang, Z. Liu, Investigation on microwave absorption properties for multiwalled carbon nanotubes/Fe/Co/Ni nanopowders as lightweight absorbers, J. Phys. Chem. C 115 (2011) 14025-14030.

13 J. Liu, J. Cheng, R. Che, J. Xu, M. Liu, Z. Liu, Synthesis and microwave absorption properties of yolk–shell microspheres with magnetic iron oxide cores and hierarchical copper silicate shells, ACS Appl. Mater. Inter. 5 (2013) 2503-2509.

14 C. Luo, T. Jiao, Y. Tang, J. Kong, Excellent electromagnetic wave absorption of iron-containing SiBCN ceramics at 1158 K high-temperature, Adv. Eng. Mater. 20 (2018) 1701168.

15 W. L. Song, X. T. Guan, L. Z. Fan, Y. B. Zhao, W. Q. Cao, C. Y. Wang, M. S. Cao, Strong and thermostable polymeric graphene/silica textile for lightweight practical microwave absorption composites, Carbon 100 (2016) 109-117.

16 H. Abbasi, M. Antunes, J. I. Velasco, Recent advances in carbon-based polymer nanocomposites for electromagnetic interference shielding, Prog. Mater. Sci. 103 (2019) 319-373.

17 A. N. Fouda, M. D. El Shazly, A. A. Almaqwashi, Facile and scalable green synthesis of N-doped graphene/CNTs nanocomposites via ball milling, Ain Shams Eng. J. 12(1) (2021) 1017-1024.

18 A. Maleki, S. Gharibi, K. Valadi, R. Taheri-Ledari, Pumice-modified cellulose fiber: an environmentally benign solid state hybrid catalytic system for the synthesis of 2,4,5-triarylimidazole derivatives, J. Phys. Chem. Solids 142 (2020) 109443.

19 A. Maleki, R. Taheri-Ledari, R. Ghalavand, R. Firouzi-Haji, Palladium-decorated *o*-phenylenediamine-functionalized Fe_3O_4/SiO_2 magnetic nanoparticles: a promising solid-state catalytic system used for Suzuki–Miyaura coupling reactions, J. Phys. Chem. Solids 136 (2020) 109200.

20 A. Maleki, Green oxidation protocol: selective conversions of alcohols and alkenes to aldehydes, ketones and epoxides by using a new multiwall carbon nanotube-based hybrid nanocatalyst via ultrasound irradiation, Ultrason. Sonochem. 40 (2018) 460-464.

21 A. Maleki, One-pot multicomponent synthesis of diazepine derivatives using terminal alkynes in the presence of silica-supported superparamagnetic iron oxide nanoparticles, Tetrahedron Lett. 54(16) (2013) 2055-2059.

22 A. Maleki, Fe_3O_4/SiO_2 nanoparticles: an efficient and magnetically recoverable nanocatalyst for the one-pot multicomponent synthesis of diazepines, Tetrahedron 68(38) (2012) 7827-7833.

23 A. Maleki, M. Aghaei, Ultrasonic assisted synergetic green synthesis of polycyclic imidazo (thiazolo) pyrimidines by using Fe_3O_4@clay core-shell, Ultrason. Sonochem. 38 (2017) 585-589.

24 A. Maleki, J. Rahimi, O. M. Demchuk, A. Z. Wilczewska, R. Jasiński, Green in water sonochemical synthesis of tetrazolopyrimidine derivatives by a novel core-shell magnetic nanostructure catalyst, Ultrason. Sonochem. 43 (2018) 262-271.

25 A. Maleki, M. Aghaei, Sonochemical rate enhanced by a new nanomagnetic embedded core/shell nanoparticles and catalytic performance in the multicomponent synthesis of pyridoimidazoisoquinolines. Ultrason. Sonochem. 38 (2017) 115-119.
26 N. Kostoglou, C. W. Liao, C. Y. Wang, J. N. Kondo, C. Tampaxis, T. Steriotis, C. Mitterer, Effect of Pt nanoparticle decoration on the H_2 storage performance of plasma-derived nanoporous graphene, Carbon 171 (2021) 294-305.
27 I. M. Afanasov, O. I. Lebedev, B. A. Kolozhvary, A. V. Smirnov, G. Van Tendeloo, Nickel/carbon composite materials based on expanded graphite, New Carbon Mater. 26(5) (2011) 335-340.
28 B. Li, W. Dong, Y. Ren, A. Feng, Preparation and characterization of spherical nickel-doped carbonized resin as hydrogenation catalysts: II. Thermal decomposition of resin and preparation of metal-doped catalysts with different nickel loadings, Carbon 45(6) (2007) 1219-1225.
29 A. Sharma, H. Nakagawa, K. Miura, Uniform dispersion of Ni nanoparticles in a carbon based catalyst for increasing catalytic activity for CH_4 and H_2 production by hydrothermal gasification, Fuel 85(17-18) (2006) 2396-2401.
30 M. Zieliński, R. Wojcieszak, S. Monteverdi, M. Mercy, M. Bettahar, Hydrogen storage in nickel catalysts supported on activated carbon, Int. J. Hydrog. Energy 32(8) (2007) 1024-1032.
31 H. Keqiang, Y. Liming, S. Leimei, A. Kang, A. Yoshinori, Z. Xinluo, Doping effect of single-wall carbon nanotubes on the microwave absorption properties of nanocrystalline barium ferrite, Jpn. J. Appl. Phys. 49 (12R) (2010) 125101.
32 X. Gui, K. Wang, J. Wei, R. Lü, Q. Shu, Y. Jia, C. Wang, H. Zhu, D. Wu, Microwave absorbing properties and magnetic properties of different carbon nanotubes, Sci. China, Ser. A: Technol. Sci. 52 (2009) 227-231.
33 D. D. L. Chung, Materials for electromagnetic interference shielding, Mater. Chem. Phys. (2020) 123587.
34 X. X. Wang, J. C. Shu, W. Q. Cao, M. Zhang, J. Yuan, M. S. Cao, Eco-mimetic nanoarchitecture for green EMI shielding, Chem. Eng. J. 369 (2019) 1068-1077.
35 L. Wang, X. Shi, J. Zhang, Y. Zhang, J. Gu, Lightweight and robust rGO/sugarcane derived hybrid carbon foams with outstanding EMI shielding performance, J. Mater. Sci. Technol. 52 (2020) 119-126.
36 L.-L. Wang, B.-K. Tay, K.-Y. See, Z. Sun, L.-K. Tan, D. Lua, Electromagnetic interference shielding effectiveness of carbon-based materials prepared by screen printing, Carbon 47 (2009) 1905–1910.
37 Y. Huang, Z. Xu, J. Shen, Dispersion of magnetic metals on expanded graphite for the shielding of electromagnetic radiations, Appl. Phys. Lett. 90 (2007) 133117.
38 G. R. Amiri, M. H. Yousefi, M. R. Abolhassani, S. Manouchehri, M. H. Keshavarz, S. Fatahian, Magnetic properties and microwave absorption in Ni–Zn and Mn–Zn ferrite nanoparticles synthesized by low-temperature solid-state reaction, J. Magn. Magn. Mater. 323 (2011) 730–734.
39 L. Yan, J. Wang, Y. Ye, Z. Hao, Q. Liu, F. Li, Broadband and thin microwave absorber of nickel–zinc ferrite/carbonyl iron composite, J. Alloys Compd. 487 (2009) 708–711.
40 S. P. Gairola, V. Verma, V. Pandey, R. L. P. Purohit, R. K. Kotnala, Modified composition of cobalt ferrite as microwave absorber in X-band frequencies, Integr. Ferroelectr. 119 (2010) 151-156.
41 K. Praveena, K. Sadhana, H. S. Virk, Structural and magnetic properties of Mn-Zn ferrites synthesized by microwave-hydrothermal process, Solid-State Phenom. 232 (2015) 45-64.
42 X. Zhang, W. Sun, Microwave absorbing properties of double-layer cementitious composites containing Mn–Zn ferrite, Cem. Concr. Compos. 32 (2010) 726–730.
43 R. Kumar, S. Kumar, S. Dhakate, Nickel nanoparticles embedded in carbon foam for improving electromagnetic shielding effectiveness, Appl. Nanosci. 5 (2014) 553-561.
44 A. Ohlan, K. Singh, N. Gandhi, A. Chandra, S. K. Dhawan, Microwave absorption properties of $NiCoFe_2O_4$-graphite embedded poly(*o*-phenetidine) nanocomposites, AIP Adv. 1 (2014) 032157.
45 E. De Fazio, P. G. Bercoff, S. E. Jacobo, Electromagnetic properties of manganese-zinc ferrite with lithium substitution, J. Magn. Magn. Mater. 323 (2011) 2813-2817.
46 X. Gui, K. Wang, J. Wei, R. Lü, Q. Shu, Y. Jia, C. Wang, H. Zhu, D. Wu, Microwave absorbing properties and magnetic properties of different carbon nanotubes, Sci. China, Ser. A: Technol. Sci. 52 (2009) 227-231.
47 M. S. Ruiz, P. G. Bercoff, S. E. Jacobo, Shielding properties of CuNiZn ferrite in the radiofrequency range, Ceram. Int. 39 (2013) 4777–4782.
48 S. E. Jacobo, P. G. Bercoff, Structural and electromagnetic properties of yttrium-substituted Ni-Zn ferrites, Ceram. Int. 42 (2016) 7664-7668.
49 S. E. Jacobo, P. G. Bercoff, C. A. Herme, L. A. Vives, Sr hexaferrite/Ni ferrite nanocomposites: magnetic behavior and microwave-absorbing properties in the X-band, Mater. Chem. Phys. 157 (2015) 124-129.
50 V. Panwar, R. M. Mehra, J. O. Park, S. H. Park, Dielectric analysis of high-density polyethylene-graphite composites for capacitor and EMI shielding application, J. Appl. Polym. Sci., 125(S1) (2012) E610-E619.
51 S. S. Pattanayak, S. H. Laskar, S. Sahoo, Microwave absorption study of dried banana leaves-based single-layer microwave absorber, Int. J. Microw. Wirel. Technol. 13(2) (2021) 154-163.
52 J. Wu, D. D. L. Chung, Pastes for electromagnetic interference shielding, J. Electron. Mater., 34(9) (2005) 1255-1258.

53 Y. Liu, J. Zeng, D. Han, K. Wu, B. Yu, S. Chai, Q. Fu, Graphene enhanced flexible expanded graphite film with high electric, thermal conductivities and EMI shielding at low content, Carbon 133 (2018) 435-445.
54 G. N. Glavee, K. J. Klabunde, C. M. Sorensen, G. C. Hadjipanayis, Borohydride reduction of nickel and copper ions in aqueous and nonaqueous media. Controllable chemistry leading to nanoscale metal and metal boride particles, Langmuir 10 (1994) 4726–4730.
55 M. Gong, D. Y. Wang, C. C. Chen, A mini review on nickel-based electrocatalysts for alkaline hydrogen evolution reaction, Nano Res. 9 (2015) 28–46.
56 D. S. Hall, D. J. Lockwood, C. Bock, B. R. MacDougall, Nickel hydroxides and related materials: a review of their structures, synthesis and properties, Proc. R. Soc. A 471 (2017) 20140792.
57 I. L. Rittner, W. G. Fano, Design and evaluation of a measurement procedure to obtain the electric permittivity and the magnetic permeability, Elektron: Ciencia y Tecnología en la Electrónica de Hoy 2(1) (2018) 30-38.
58 P. Saini, V. Choudhary, B. P. Singh, R. B. Mathur, S. K. Dhawan, Polyaniline–MWCNT nanocomposites for microwave absorption and EMI shielding. Mater. Chem. Phys. 113 (2009) 919–926.
59 P. Saini, V. Choudhary, B. P. Singh, R. B. Mathur, S. K. Dhawan, Enhanced microwave absorption behavior of polyaniline-CNT/polystyrene blend in 12.4–18.0 GHz range, Synth. Met. 161 (2011) 1522–1526.
60 A. C. Ferrari, J. F. Robertson, Interpretation of Raman spectra of disordered and amorphous carbon, Phys. Rev. B, 61 (2000) 14095.
61 M. A. Pimenta, G. Dresselhaus, M. S. Dresselhaus, L. G. Cancado, A. Jorio, R. Saito, Studying disorder in graphite-based systems by Raman spectroscopy, Phys. Chem. Chem. Phys. 9 (2007) 1276–1290.
62 J. Liu, Q. Li, Y. Zou, Q. Qian, Y. Jin, G. Li, K. Jiang, S. Fan, The dependence of graphene Raman D-band on carrier density, Nano Lett. 13 (2013) 6170–6175.
63 R. Kumar, H. K. Choudhary, A. V. Anupama, A. V. Menon, S. P. Pawar, S. Bose, B. Sahoo, Nitrogen doping as a fundamental way to enhance the EMI shielding behavior of cobalt particle-embedded carbonaceous nanostructures, New J. Chem. 43(14) (2019) 5568-5580.
64 X. He, W. Zhong, C. T. Au, Y. Du, Size dependence of the magnetic properties of Ni nanoparticles prepared by thermal decomposition method, Nanoscale Res. Lett. 8 (2013) 446.
65 K. Shafi, A. Gedanken, R. Prozorov, J. Balogh, Sonochemical preparation and size-dependent properties of nanostructured $CoFe_2O_4$ particles, Chem. Mater. 10 (1998) 3445–3450.
66 G. G. Couto, J. J. Klein, W. H. Schreiner, D. H. Mosca, A. J. A. de Oliveira, A. J. G. Zarbin, Nickel nanoparticles obtained by a modified polyol process: synthesis, characterization, and magnetic properties, J. Colloid Interface Sci. 311 (2007) 461–468.
67 M. Koledintseva, P. C. Ravva, J. Drewniak, A. A. Kitaitsev, A. A. Shinko, Engineering of ferrite-graphite composite media for microwave shields. IEEE International Symposium on Electromagnetic Compatibility. EMC 2006, Portland OR, USA, 2006, 598-602.
68 Y. L. Huang, S. M. Yuen, C. C. M. Ma, C. Chuang, K. Yu, C. Teng, H. Tien, Y. C. Chiu, S. Wu, S. H. Liao, Morphological, electrical, electromagnetic interference (EMI) shielding, and tribological properties of functionalized multi-walled carbon nanotube/polymethyl methacrylate (PMMA) composites, Compos. Sci. Technol. 69 (2009) 1991–1996.